

BEHAVIOR OF INCLUSIONS WITH DIFFERENT VALUE AND ORIENTATION OF TOPOLOGICAL DIPOLES IN FERROELECTRIC SMECTIC FILMS

P. V. Dolganov^{a}, V. K. Dolganov^a, P. Cluzeau^b*

^a*Institute of Solid State Physics, Russian Academy of Sciences
142432, Chernogolovka, Moscow Region, Russia*

^b*Université Bordeaux I, Centre de Recherche Paul Pascal, CNRS
33600, Pessac, France*

Received February 24, 2009

Cholesteric droplets in ferroelectric free-standing films with tunable anchoring on the droplet boundary are investigated. A droplet and satellite topological defect(s) form a topological dipole. We obtained droplets with different angles α between two radial lines from the droplet center to $-1/2$ topological defects. Droplets with parallel dipoles form linear chains in which the interparticle distances decrease with increasing the defect angle α . For the first time, the dependence of the interparticle distance on the angle between topological defects was measured. We can adjust the magnitude and orientation of topological dipoles formed by the droplets. For the first time, the droplets with antiparallel topological dipoles were prepared in a smectic film. Interaction of the droplets with parallel and antiparallel dipoles differs drastically. Formation of antiparallel dipoles leads to a decomposition of the droplet pairs and chains of droplets. Our observations may be used to change the magnitude, anisotropy of the interparticle interaction, and structures from inclusions in liquid crystal media.

PACS: 61.30.Jf, 61.30.Gd, 81.16.Dn

1. INTRODUCTION

Self-organization of inclusions in liquid crystals [1–3] opens new possibilities in engineering of microstructures in condensed matter [1–5]. Inclusions interact via the elastic deformation of liquid crystal host media [1–3, 6–10]. Deformation of the liquid crystal occurs due to a fixed orientation of molecules at the inclusion boundary. The anchoring conditions determine the anisotropy, strength of the interparticle interaction, and structures formed by the inclusions. It was found recently [11, 12] that the chirality of the liquid crystal may drastically change the position of the topological defects and molecular orientation on the boundary of droplets embedded in free-standing smectic films [13, 14]. This result demonstrates that both interaction and organization of inclusions can be controllable.

Smectic layers in free-standing films are parallel to

the free surfaces. Every layer is a two-dimensional (2D) ordered liquid. In the ferroelectric smectic- C^* ($\text{Sm}C^*$) phase [15], the nematic director \mathbf{n} [15] is tilted with respect to the layer normal. The projections of \mathbf{n} onto the smectic layer planes form a 2D field of molecular orientation or the so-called \mathbf{c} -director field. The layer ferroelectric polarization \mathbf{P} is perpendicular to the tilt plane. In the $\text{Sm}C^*$ films, droplets nucleate with planar anchoring [16], i.e., the \mathbf{c} -director field near the droplets orients parallel to the droplet boundary. A droplet with strong anchoring is equivalent to a topological defect with the topological charge $S = +1$ [6]. To preserve the topological neutrality of the system, the droplet nucleates with the accompanying topological defect bearing the topological charge $S = -1$. The droplet and the defect with topological charges of opposite sign form a topological dipole. For many years only dipolar inclusions with $S = -1$ topological defects and parallel dipole orientation were observed in ferroelectric films. Their interaction and self-assembly have been investigated. No procedures for preparing dipolar

*E-mail: pauldol@issp.ac.ru

inclusions of other types and inclusions with antiparallel dipoles have been reported.

In this paper, the dipolar droplets both with one $S = -1$ and with two $S = -1/2$ defects, with parallel and antiparallel orientation of topological dipoles, are obtained. The investigations were performed on a pure chiral compound and on its mixture with racemate. In polar films, interparticle interaction is manipulated by changing the temperature, polarization, and droplet size. In a material with a fixed handedness, droplets with the opposite \mathbf{c} -director rotation around the droplet were obtained. Droplets with parallel topological dipoles are attracted in the direction parallel to their dipoles and form droplet chains. Droplets with antiparallel topological dipoles are attracted in a perpendicular direction. The interparticle distances in the chains formed by droplets decrease with increasing the defect angle between two $S = -1/2$ topological defects.

2. EXPERIMENT

Most experiments were carried out on free-standing films of chiral S-4'-undecyloxybiphenyl-4-yl 4-(methylheptyloxy)benzoate (11BSMHOB) forming the ferroelectric SmC^* phase [17]. Some measurements were made on a mixture of chiral 11BSMHOB (25 % wt) with racemic 11BSMHOB. Free-standing films were prepared by drawing a small amount of the compound in the SmC^* phase across a circular hole (4 mm in diameter) in a thin glass plate. The film thickness L was determined from the optical reflectivity in "backward" geometry [13]. In thick films, cholesteric droplets nucleate in the vicinity of the bulk smectic-cholesteric transition temperature T_C . In thin films ($L < 50$ nm), the nucleation is shifted to higher temperatures. Below T_C , the droplets are transformed into smectic islands whose thickness is larger than the thickness of the film. The droplets and the textures of the film were observed using an optical microscope in reflection mode. Observations between crossed polarizers (polarized reflected light microscopy, PRLM) and in depolarized reflected light microscopy (DRLM) [18] allow determining the orientation of the \mathbf{c} -director in the films.

3. RESULTS AND DISCUSSION

Figure 1a shows a droplet at a low temperature. Near the temperature of the transition of the cholesteric phase in the droplets to the smectic phase, the droplets have one $S = -1$ topological defect on their boundary. The orientation of the \mathbf{c} -director field on the bound-

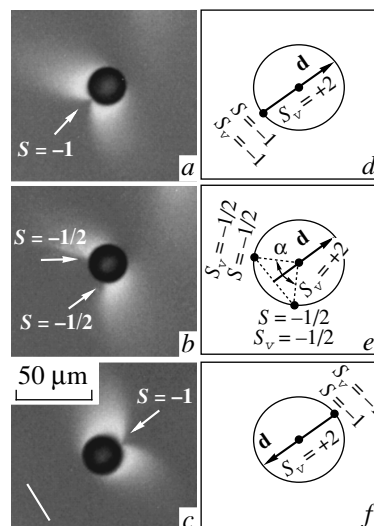


Fig. 1. Reorientation of an $S = -1$ topological defect to the opposite side of the droplet. The $S = -1$ topological defect (a) dissociates in two $S = -1/2$ topological defects (b). They move in opposite directions over the droplet boundary and join into an $S = -1$ defect on the opposite side of the droplet (c). The positions of topological defects are shown with white arrows in (a), (b), and (c). Solid arrows in (d), (e), and (f) show the topological dipole moments. S and S_v are the topological charges of real and virtual defects. The white line in the lower left part of (c) shows the orientation of the \mathbf{c} -director in the dark regions. α is the angle between topological defects. The photographs were taken in DRLM

ary of the droplet is planar. It was found recently that the direction of the \mathbf{c} -director orientation on the droplet boundary can be changed [11]. On heating, the $S = -1$ satellite surface defect (Fig. 1a) may split into two $S = -1/2$ defects (Fig. 1b) moving over the droplet boundary in opposite directions. The moving $S = -1/2$ defects rotate the \mathbf{c} -director field on the droplet boundary by 180° . In relatively thick films ($L > 30$ nm), $S = -1/2$ defects join on the opposite side of the droplet and again form a dipolar droplet with one $S = -1$ topological defect (Fig. 1c). By changing temperature, droplets with different defect angles α between the $S = -1/2$ defects, seen from the droplet center, can be obtained.

According to the electromagnetic analogy [6], a droplet with strong anchoring for the \mathbf{c} -director can be regarded as a set of real and virtual topological defects. If a real $S = -1$ defect is located in the smectic film, the virtual defect is the image of the real $S = -1$ defect. A droplet with an $S = -1$ defect on the droplet

boundary is equivalent to a real $S = -1$ defect, a virtual $S_V = -1$ defect at the location of the $S = -1$ defect, and a virtual $S_V = +2$ defect in the center of the droplet (Fig. 1d). For the droplet in Fig. 1b, two virtual $S_V = -1/2$ defects should be added at the locations of real $S = -1/2$ defects and a virtual $S_V = +2$ defect should be placed in the center of the droplet (Fig. 1e). The topological dipole moment of the droplet is $\mathbf{d} = \sum S_i \mathbf{r}_i$, where the strengths S_i of both real and virtual topological defects are taken into account, and \mathbf{r}_i are the positions of real and virtual defects. In a dipolar droplet with an $S = -1$ defect, the topological dipole d equals $d = 2R$, where R is the droplet radius. The dipole moment vector orients from the point defect to the droplet center (Fig. 1d). After splitting the $S = -1$ defect in two $S = -1/2$ defects, the dipole moment becomes $d = 2R \cos \alpha/2$. The dipole moment decreases when defects with $S = -1/2$ move over the droplet boundary (Fig. 1b,e), passes through zero at $\alpha = \pi$ (quadrupolar configuration), and then changes its direction to the opposite (Fig. 1f).

We first consider the cause of the formation of one $S = -1$ or two $S = -1/2$ defects and their motion over the droplet boundary. Starting from paper [6], only quadratic elasticity was considered in describing the \mathbf{c} -director configuration near the droplet. In chiral SmC* films, the energy of the system $F = F_q + F_l$ includes the quadratic (F_q) and linear (F_l) elasticity [19–21],

$$F_q = \frac{1}{2}K \int [(\nabla \cdot \mathbf{c})^2 + (\nabla \times \mathbf{c})^2] dx dy dz, \quad (1)$$

$$F_l = \frac{1}{2}K\lambda \int (\nabla \times \mathbf{c})_z dx dy dz, \quad (2)$$

where splay K_S and bend K_B elastic constants are assumed equal ($K_S = K_B = K$, the one-constant approximation). The term $(\nabla \times \mathbf{c})_z$ has opposite sign for clockwise and counterclockwise rotation of the \mathbf{c} -director. Linear elasticity is the reason for the different position of the topological defects on the droplet boundary [16].

Position of the topological defect on the boundary of a circular inclusion (Fig. 2a,b) was calculated in [22, 23] with both quadratic and linear elasticity of the film taken into account. The energy of the topological defect is proportional to the square of its strength S^2 . The elastic energy F_q favors the formation of two $S = -1/2$ defects with a large distance between them, $\alpha = \pi$ (quadrupolar configuration). But the linear elasticity favors another configuration, because the energy F_l has opposite signs for clockwise and counterclockwise rotations of the \mathbf{c} -director around the inclusion.

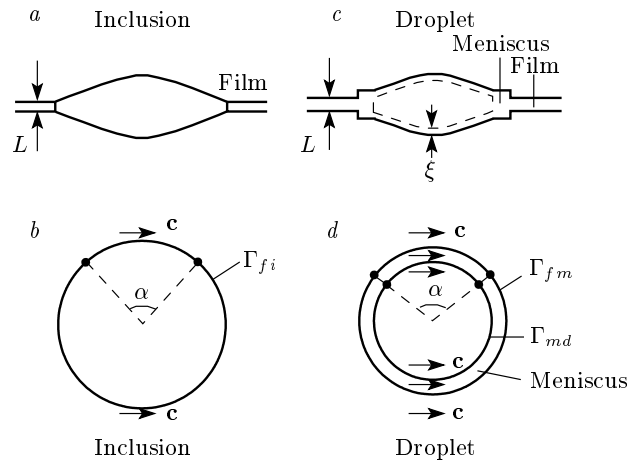


Fig. 2. Schematic representation of the inclusion structure in a smectic film. Figs. a and b show an inclusion with a simple structure. α is the angle between topological defects. Γ_{fi} is the boundary between the film and the inclusion. Figs. c and d represent a droplet with meniscus and surface smectic layers. L is the thickness of the film, Γ_{fm} is the boundary between the film and the meniscus, Γ_{md} is the boundary between the meniscus and the droplet, and ξ is the correlation length of surface smectic ordering

The free energy F_l is a total derivative and can be expressed as an integral over the outer boundary Γ_0 of the film and the inner contour Γ_{fi} between the film and the inclusion

$$F_l = \frac{K\lambda}{2} \int_{\Gamma_0 + \Gamma_{fi}} d\mathbf{l} \cdot \mathbf{c} dz.$$

We consider the case where

$$\int_{\Gamma_0} d\mathbf{l} \cdot \mathbf{c}$$

is independent of the position of the topological defects on the droplet boundary, for instance, the uniform orientation of the \mathbf{c} -director far away from droplet, that is,

$$\int_{\Gamma_0} d\mathbf{l} \cdot \mathbf{c} = 0.$$

An inclusion with a single boundary between the film and the inclusion was considered in [22, 23] (Fig. 2a,b). In this case, the energy of the film due to the linear elasticity is $F_{lf} = K\lambda LR(\alpha - \pi)$. This equation is written for counterclockwise rotation of the \mathbf{c} -director along the inclusion boundary outside the defect angle. For definiteness, we consider $\lambda > 0$. The elastic energy F_{lf}

favors the dipolar configuration ($\alpha = 0$), whereas F_q favors the quadrupolar configuration ($\alpha = \pi$). The competition between quadratic (F_q) and linear (F_l) elasticity can lead to an intermediate position of topological defects, $0 < \alpha < \pi$ [22, 23]. In this model, the behavior of topological defects is independent of the interior inclusion structure. This case can be realized for solid inclusions at high temperature when the meniscus between the inclusion and the film is small and only the energy of the free-standing film can be taken into account.

The structure of the droplets is not so simple as shown in Fig. 2*a,b* and the behavior of the droplets in the film depends on their internal structure. In particular, the droplet boundary is encircled by a meniscus (Fig. 2*c,d*) with the thickness larger than the surrounding film. Surface ordering leads to the formation of smectic layers on the surface of the droplet. Their thickness is determined by the smectic correlation length ξ [14]. The elastic energy of the droplet and the meniscus lead to an additional competition between the energy of the film and the droplet [12]. For the configuration corresponding to negative elastic energy $F_{lf} < 0$ of the whole film, $(\nabla \times \mathbf{c})_z > 0$ in some region around the droplet. On a certain part of the droplet boundary, the \mathbf{c} -director rotates in the direction (counterclockwise in Fig. 2*d*) opposite to the favorable \mathbf{c} -director rotation due to the linear elasticity ($(\nabla \times \mathbf{c})_z < 0$ for clockwise rotation). The direction of the \mathbf{c} rotation outside the droplet is transmitted to the \mathbf{c} -director rotation in the meniscus and to the surface smectic layers in the droplet (Fig. 2*d*). The competition between the energies of quadratic elasticity F_q and the linear elasticity of the film F_{lf} , the droplet F_{ld} , and the meniscus F_{lm} leads to complex droplet behavior depending on the temperature, chirality, and droplet size. The position of the topological defects (i.e., the angle α) and consequently the interparticle interaction depends on the linear elasticity λ , the size of the inclusion R and the meniscus, and the smectic correlation length ξ . In turn, the smectic correlation length ξ depends on temperature. The size of the meniscus depends on the temperature and film thickness. In our case, the surface anchoring energy W [11, 24] is sufficiently large to dictate the planar \mathbf{c} -director orientation on the droplet boundary outside the topological defect. However, competition between quadratic and linear elasticity leads to a 180° -change of the \mathbf{c} -director orientation in the core of the topological defect upon its moving. After the reorientation, the \mathbf{c} -director remains planar. Therefore, using droplets of different sizes and changing the chirality, temperature, and film thickness,

droplets with different defect angle α , with the parallel and antiparallel topological dipole orientation, can be prepared in smectic films.

3.1. Inclusions with parallel topological dipoles

Interaction between inclusions at both large and small distances depends on the defect angle α . According to theory [6], the inclusions interact via the elastic deformation of the \mathbf{c} -director field. At large distances, two droplets interact as dipoles with the topological moments $d_1 = 2R_1 \cos \alpha_1/2$ and $d_2 = 2R_2 \cos \alpha_2/2$. The pair dipolar interaction energy E_d is given by [6, 25]

$$E_d = \pm \frac{2\pi K d_1 d_2}{R^2} \cos 2\varphi, \quad (3)$$

where φ is the angle between the topological moment of one of the droplets and the direction to the other droplet. The sign of the energy depends on the relative orientation of the topological dipoles (the minus sign for parallel dipoles and the plus sign for antiparallel dipoles in Eq. (3)). In what follows, we adopt the notation in Ref. [26] and call the droplets with the line of droplet centers parallel ($\varphi = 0$) and perpendicular ($\varphi = 90^\circ$) to the topological dipole, respectively, the longitudinal and lateral droplets.

Figure 3 shows the process of chaining of longitudinal droplets with parallel topological dipoles. They are attracted at large separations. At small separations, the interaction becomes repulsive. The droplets form a straight chain oriented perpendicular to the direction of the far-field \mathbf{c} -director. The defects lie between the droplets and prevent the droplets from coalescence. We observed that droplets with a defect angle $\alpha < 60^\circ$ form line chains. Figure 4 shows the interdroplet spacing in chains versus the defect angle α . As the defect angle increases, the repulsive interaction between the droplets decreases and the droplets approach each other. Therefore, by changing the position of the topological defects, we are able to change the interaction of the droplets at large and small separations.

3.2. Inclusions with antiparallel topological dipoles

We found that the temperature T_R of the reorientation of topological defects (Fig. 1) depends on the droplet size. Topological defects in larger droplets reorient at higher temperature. In a temperature interval ΔT_R that depends on the film thickness, we obtained droplets with the antiparallel dipole orientation. Figure 5*a* shows the droplets at low temperature. Their

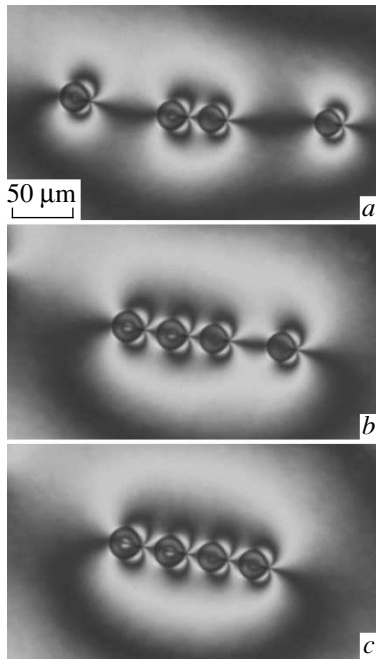


Fig. 3. Dipolar droplets with parallel topological dipole moments attract each other and form a stable line chain. Photos *b* and *c* were made in 32s and 50s after photo *a*

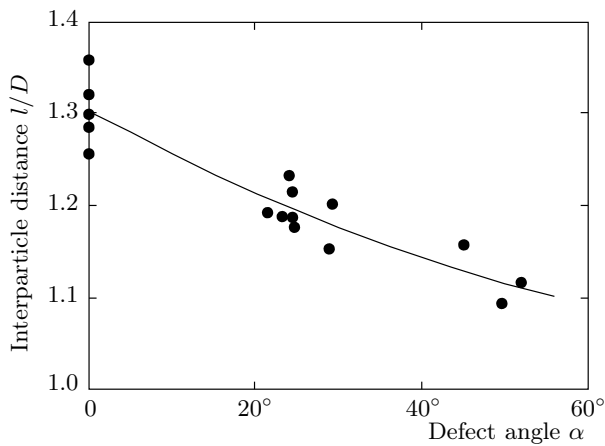


Fig. 4. The interparticle distance in chains decreases with increasing the defect angle α ; l is the distance between droplet centers and D is the droplet diameter

topological dipoles are oriented parallel to each other. Figure 5*b* shows the droplets of different size. On heating, reorientation occurred in the smaller droplet (Fig. 5*b*), and its topological defect oriented in the direction opposite to that at low temperature. In the larger droplet, the orientation of the defect and the

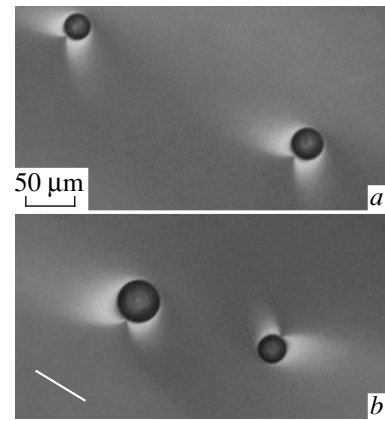


Fig. 5. Cholesteric droplets in SmC^* films. (a) Topological dipoles associated with the droplets orient in the same direction. (b) Topological dipoles associated with the droplets orient in antiparallel directions. The photographs were taken in DRLM. The white line in *b* shows the orientation of the c-director in the dark regions

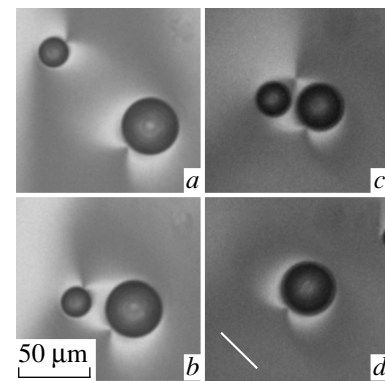


Fig. 6. Lateral dipolar droplets with antiparallel topological dipole moments (a) attract and approach each other (b). Pictures *a* and *b* show the droplets with defects on the boundaries of the droplets. Frame *c* shows droplets with a defect on the boundary of the droplet (the larger droplet) and a defect in the bulk. The droplets attract, come in contact with each other, and coalesce into a single droplet. The droplet in Fig. 6*d* was formed from two droplets in Fig. 6*c*. The photographs were taken in DRLM. The white line in *d* shows the orientation of the c-director in the dark regions

topological dipole remain unchanged. This procedure is used to produce droplets with antiparallel dipoles.

Lateral droplets with antiparallel topological dipoles attract each other and the separation between

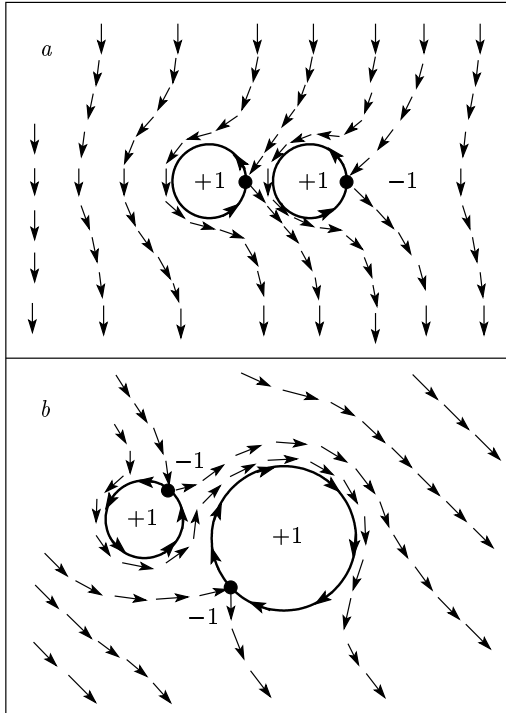


Fig. 7. Schematic representation of the \mathbf{c} -director field near droplets with parallel (*a*) and antiparallel (*b*) topological dipole orientations. Droplets with parallel dipoles are separated by the topological defects that stabilize the interparticle distances. The numbers -1 and $+1$ denote the topological charge of the defects and the topological charge associated with the droplets

the droplets decreases (Fig. 6*a,b*). Figure 6*a,b* shows the droplets with surface defects. On the contrary, in Fig. 6*c*, the smaller droplet does not have an $S = -1$ defect on its boundary but is accompanied by a bulk $S = -1$ defect located at some distance from the droplet. In both cases (Fig. 6*b,c*), there are no defects on the line connecting the droplet centers. The droplets come in contact and coalesce into a single droplet. The droplet in Fig. 6*d* results from the coalescence of two droplets shown in Fig. 6*c*. We note that the orientation of the topological dipole moment of the droplet in Fig. 6*d* coincides with the dipole moment of the larger droplet in Fig. 6*c*. The reason is that the reorientation in larger droplets occurs at higher temperature.

Figure 7 shows a schematic representation of the \mathbf{c} -director field near droplets with parallel (*a*) and antiparallel (*b*) topological dipoles. In the chains formed by the droplets with parallel dipoles (Figs. 3, 7*a*), the droplets are separated by topological defects, which stabilize the chain structure and prevent droplet co-

alescence. For the antiparallel orientation of dipoles, the droplets are not separated by topological defects. The droplets do not form stable structures, they attract each other, and coalesce.

3.3. Reorientation of topological defects in the droplet structures

The transition of the $S = -1$ topological defect to the opposite side of the droplets occurs not only in single droplets but also in chains formed by droplets. In the latter case, the transition occurs at approximately the same temperature T_R as in single droplets. Behavior of the chains depends on the droplet size. If the chain is formed by droplets of equal size, reorientation of the topological defects occurs simultaneously in all droplets. Both the decomposition of the chain to single droplets and approach of the droplets to each other with coalescence may occur. If the sizes of droplets in the chain differ, two different transformations are found on heating and cooling.

(1) The point topological defects between the droplets are located at the boundary of the larger droplet (Fig. 8). Pairs of droplets are stable structures above (Fig. 8*a*) and below (Fig. 8*d*) the temperature range of the reorientation of topological defects.

(a) On cooling (Fig. 8*a,b,c*), the transformation starts in the larger droplet (Fig. 8*b*). Two $S = -1/2$ defects move along the droplet boundary as in an isolated droplet. But droplets with opposite directions of the topological dipoles are typically not formed. As the defect angle increases, the droplets approach each other (Fig. 8*b*). When the defect angle becomes larger than 60° , the two droplets, as a rule, coalesce into a single droplet. The droplet in Fig. 8*c* is formed from two droplets in Fig. 8*b*.

(b) On heating (Fig. 8*d,e,f*), the transformation starts in the smaller droplet (Fig. 8*e*). Two half-defects move over the boundary of the smaller droplet and form an $S = -1$ surface defect on the opposite side of the droplet. Droplets with opposite directions of the topological dipoles are formed. Longitudinal droplets with antiparallel topological dipoles repel from each other and become widely separated (Fig. 8*f*).

(2) If the point topological defect between the droplets is located on the surface of the smaller droplet, the behavior of the droplet pairs is opposite to that described in item (1).

(a) On cooling, the droplet pair breaks down into two isolated droplets with antiparallel topological dipoles.

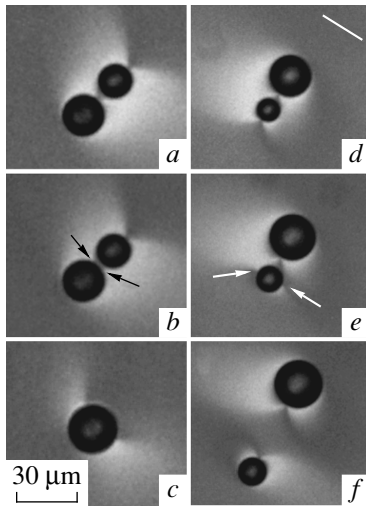


Fig. 8. Reorientation of the topological defects in droplet pairs. The droplet behavior depends on whether the film is cooled (*a-c*) or heated (*d-f*) and on the relative position of the larger and smaller inclusions in the chain. (*a-c*) Reorientation of the defects on the boundary of the larger droplet (*b*) leads to coalescence of the droplets. (*d-f*) Reorientation of the defects on the boundary of the smaller droplet (*e*) leads to a decomposition of the pair into single droplets (*f*). Arrows show the position of $S = -1/2$ defects on the droplet boundary during the reorientation. The photographs were taken in DRLM. The white line in *d* shows the orientation of the *c*-director in the dark regions

(*b*) On heating, the droplets approach each other and coalesce into a single droplet.

The above experimental observations of droplet interaction are qualitatively consistent with the elastic theory of interparticle interaction [6, 27] and dynamic simulation of droplet interaction [26].

Droplets self-organize in chains and pairs of droplets above and below the temperature range of the reorientation of topological defects. The behavior of the chains during the defect reorientation is rather complicated. Droplets approach each other if the topological defect between them reorients. When the defect angle becomes too large, the droplets coalesce. Droplets are moving apart if the defect not located between them reorients. Similar behavior is observed in chains of droplets.

In summary, using the reorientation of the surface topological defect on the droplet boundary in ferroelectric films, we prepared droplets with different values of topological dipoles, with parallel and antiparallel orientation of topological dipoles. Longitudinal

droplets with parallel dipoles attract one another and come together to form a stable line chain. Lateral droplets with antiparallel dipoles attract, approach one another, and coalesce. The interparticle distance in the chains can be changed essentially by changing the position of defects on the droplet boundary. Change of the value and sign of the interparticle interaction can be used for manipulation of the self-organized structures of inclusions.

This work was supported in part by the RFBR (grants №№ 08-02-00827, 09-02-00098) and by the Russian Science Support Foundation. We thank A. Babeau and S. Gineste for synthesis of the liquid crystals.

REFERENCES

1. P. Poulin, H. Stark, T. C. Lubensky, and D. A. Weitz, *Science* **275**, 1770 (1997).
2. T. C. Lubensky, D. Petthey, N. Currier, and H. Stark, *Phys. Rev. E* **57**, 610 (1998).
3. P. Poulin and D. A. Weitz, *Phys. Rev. E* **57**, 626 (1998).
4. W. Russel, D. Saville, and W. Schowalter, *Colloidal Dispersions*, Cambridge Univ. Press, Cambridge, U. K. (1989).
5. C. Lapointe, A. Hultgren, D. M. Silevitch, E. Felton, D. H. Reich, and R. L. Leheny, *Science* **303**, 652 (2004).
6. D. Petthey, T. C. Lubensky, and D. R. Link, *Liq. Cryst.* **25**, 579 (1998).
7. H. Stark, *Eur. Phys. J. B* **10**, 311 (1999).
8. J.-C. Loudet, P. Barois, and P. Poulin, *Nature (London)* **407**, 611 (2000).
9. V. G. Nazarenko, A. B. Nych, and B. I. Lev, *Phys. Rev. Lett.* **87**, 075504 (2001).
10. P. V. Dolganov, H. T. Nguyen, G. Joly, V. K. Dolganov, and P. Cluzeau, *Eur. Phys. J. E* **25**, 31 (2008).
11. P. V. Dolganov, H. T. Nguyen, E. I. Kats, V. K. Dolganov, and P. Cluzeau, *Phys. Rev. E* **75**, 031706 (2007).
12. P. V. Dolganov and P. Cluzeau, *Phys. Rev. E* **78**, 021701 (2008).
13. P. Pieranski et al., *Physica A* **194**, 364 (1993).
14. W. H. de Jeu, B. I. Ostrovskii, and A. N. Shalaginov, *Rev. Mod. Phys.* **75**, 181 (2003).

15. P. G. de Gennes and J. Prost, *The Physics of Liquid Crystals*, 2nd ed., Clarendon Press, Oxford (1993).
16. P. V. Dolganov, H. T. Nguyen, G. Joly, V. K. Dolganov, and P. Cluzeau, *Europhys. Lett.* **76**, 250 (2006).
17. P. Cluzeau, M. Ismaili, A. Annakar, M. Foulon, A. Babeau, and H. T. Nguyen, *Mol. Cryst. Liq. Cryst. Sci. Technol., Sect. A* **362**, 185 (2001).
18. D. R. Link, G. Natale, R. Shao, N. A. Clark, E. Korobova, and D. M. Walba, *Science* **84**, 3665 (1999).
19. S. A. Langer and J. P. Sethna, *Phys. Rev. A* **34**, 5035 (1986).
20. J. V. Selinger, Z. G. Wang, R. F. Bruinsma, and C. M. Knobler, *Phys. Rev. Lett.* **70**, 1139 (1993).
21. R. D. Kamien and J. V. Selinger *J. Phys.: Condens. Matter* **13**, R1 (2001).
22. C. Bohley and R. Stannarius, *Eur. Phys. J. E* **23**, 25 (2007).
23. J. Fukuda, *Eur. Phys. J. E* **24**, 91 (2007).
24. A. Rapini and M. Papoular, *J. Phys. (Paris), Colloq.* **30**, C4-54 (1969).
25. P. V. Dolganov and V. K. Dolganov, *Phys. Rev. E* **73**, 041706 (2006).
26. C. Zhou, P. Yue, and J. J. Feng, *Langmuir* **24**, 3099 (2008).
27. K. S. Korolev and D. R. Nelson, *Phys. Rev. E* **77**, 051702 (2008).